Screening of magnetic fields by superconducting and hybrid shields with a circular cross-section

Screening of magnetic fields by superconducting and hybrid shields with circular cross-section

Laura Gozzelino[1,2], Michela Fracasso[1,2], Mykola Solovyov[3], Fedor Gömöry[3], Andrea Napolitano[1,2], Roberto Gerbaldo[1,2], Gianluca Ghigo[1,2], Francesco Laviano[1,2], Daniele Torsello[1,2], Mihai A Grigoroscuta[4], Gheorghe Aldica[4], Mihail Burdusel[4], Petre Badica[4]

[1] Department of Applied Science and Technology, Politecnico di Torino, Torino, Italy
[2] Istituto Nazionale di Fisica Nucleare, Sezione di Torino, Torino, Italy
[3] Institute of Electrical Engineering, Slovak Academy of Sciences, Bratislava, Slovakia
[4] National Institute of Materials Physics, Magurele, Romania

E-mail: laura.gozzelino@polito.it

Received xxxxxx
Accepted for publication xxxxxx
Published xxxxxx

Abstract

The use of superconducting (SC) materials is crucial for shielding quasi-static magnetic fields. However, the frequent requisite of space-saving solutions with high shielding performance requires the development of a 3D modelling procedure capable of predicting the screening properties for different orientations of the applied field. In this paper, we exploited a 3D numerical model based on a vector potential formulation to investigate the shielding ability of SC screens with cylindrical symmetry and a height/diameter aspect ratio close to unity, without and with the superimposition of a ferromagnetic (FM) circular shell. The chosen materials were MgB_2 and soft iron. First, the calculation outcomes were compared with the experimental data obtained on different shielding arrangements, achieving a notable agreement in both axial-field (AF) and transverse-field (TF) orientations. Then, we used the thus validated modelling approach to investigate how the magnetic mitigation properties of a cup-shaped SC bulk can be improved by the superimposition of a coaxial FM cup. Calculations highlighted that the FM addition is very efficient in enhancing the shielding factors (SFs) in the TF orientation. Assuming a working temperature of 30 K and using a layout with the FM cup protruding over the SC one, shielding factors up to 8 times greater than those of the single SC cup were attained at applied fields up to 0.15 T, reaching values equal or higher than 10^2 in the inner half of the shield. In the AF orientation, the same FM cup addition costs a modest worsening at low fields, but at the same time, it widens the applied field range, where $SF \geq 10^4$ occurs near the close extremity of the shield, up over 1 T.

Keywords: magnetic shielding, superconductor modelling, MgB_2 bulk superconductors

1. Introduction

Magnetic mitigation is essential to solving problems of electromagnetic compatibility between instruments, as well as to enable the operation of devices requiring a very low environmental field. Passive shielding arrangements, exploiting the intrinsic properties of superconducting (SC) materials, have been proved to strongly mitigate low-frequency magnetic fields [1-9] even with a magnitude,

$\mu_0 H_{appl}$, exceeding 1 Tesla [10-12].

Furthermore, improvements in superconducting shield performance have been found by superimposing one or more ferromagnetic (FM) layers [13-19] including the possibility to cloak static (DC) and alternating (AC) magnetic fields in suitably shaped SC/FM heterostructures [20-24].

Among SC materials, MgB_2 is a promising option [11, 12, 25] because the precursors are cheap, non-toxic and do not contain rare earth elements or noble metals. In addition, the low weight density of the compound makes it suited for space applications [26, 27]. Also, its long coherence length enables the fabrication of large untextured polycrystalline samples in which high current densities flow across clean grain-boundaries.

However, the fabrication of efficient magnetic shields also requires the development of i) manufacturing techniques able to provide suitably shaped objects with high and homogeneous critical current density and ii) modelling procedures able to guide the shielding devices design depending on the required working conditions. In particular, improving the shielding capability under realistic operating conditions requires a 3D modelling approach, which allows one to analyse the shielding performance for a non-uniform magnitude and various orientations of the applied magnetic field [28, 29].

With reference to the first point mentioned above, the MgB_2 feature of carrying large current across grain boundaries has fostered the development of manufacturing techniques [30-32] able to produce large MgB_2 bulks with shapes meeting specific application requirements. In our previous papers [12, 33], we reported on the possibility to get high-quality and fully machinable MgB_2 bulks by Spark Plasma Sintering of MgB_2 powders added with hexagonal BN powders. The as-sintered products can be processed with cutting tools in order to satisfy specific shape constraints. The tube- [33] and cup-shaped [12] vessels thus manufactured showed remarkably high shielding factors (SFs), even for small height/diameter aspect ratios. Therefore, they are promising prototypes to address the practical requirement of space-saving shielding solutions.

On the other hand, in the last few years several numerical techniques for modelling superconductors have been proposed with the aim to optimize magnetic device layouts [34-41]. In this context, we exploited the vector potential (**A**-V) formulation developed in [42] to predict the magnetic flux penetration in SC and SC/FM coaxial shields, when an axial magnetic field is applied [33, 43]. Taking advantage of the axisymmetric geometry of the problem, a 2D approach was implemented using the commercial software COMSOL Multiphysics® [44]. Very recently, the same method was extended to a 3D formulation and successfully applied to reproduce the experimental magnetization loops of a SC ring and a SC solenoid in a transverse field orientation [45].

In this paper, we exploited this 3D computational approach to investigate the role of a ferromagnetic shell in improving the screening ability of MgB_2 tube and cup-shaped shields. The analysis was carried out both in axial-field (AF) and transverse-field (TF) orientations. To this aim, we firstly checked the model feasibility of reproducing the magnetic flux density values measured for different shielding configurations. Next, the thus validated numerical procedure was applied to predict the screening properties of new hybrid SC/FM cup-shaped layouts. The computed results for the hybrid configurations were then compared with each other and with those with only the SC cup. With the aim to develop shielding solutions meeting the volume constrains of working environments, such as space, where the volume occupied by each devices need to be kept as low as possible, we still dealt with systems with an aspect ratio of height/average diameter close to unity. In such systems, the non-negligible field penetration through the open end(s) of the shield makes the prediction of the screening capability non-trivial [18, 43, 46].

The paper is organized as follows. Section 2 deals with the experimental details on the samples and measurements while the description of the finite-element method used for the numerical calculations is reported in section 3. Experimental and calculated magnetic flux density distributions obtained with different shielding layouts in both axial- and transverse-applied fields are compared in section 4. In section 5, the effect of the superimposition of a FM cup-shaped shield on a SC one is numerically investigated in configurations with a different relative height of the two cups. Finally, the main outcomes are summed up in section 6.

2. Experimental details

The efficiency of MgB_2 shields obtained with the innovative manufacturing process described in Ref. 33 and shaped as a hollow cylinder and cup was investigated by cooling them in zero magnetic field down to the working temperature and then by applying a slowly increasing homogenous field either parallel or perpendicular to the shield axis [12]. To this end, the shield was placed in tight thermal contact with the second stage of a cryogen-free cryocooler (see Ref. 33 for more details). The magnetic flux density was measured by means of cryogenic Ga-As Hall probes [47] located along the shield axis. The probes were always oriented to measure the component of the magnetic flux density parallel to the applied field. Likewise, the screening ability of a hybrid shield consisting of a MgB_2 hollow cylinder coaxially mounted inside a ferromagnetic tube made out of Fe ARMCO was also evaluated. This hybrid shield was suitably degaussed before each set of measurements.

The three configurations experimentally investigated (EC1, EC2 and EC3) are sketched in figure 1.

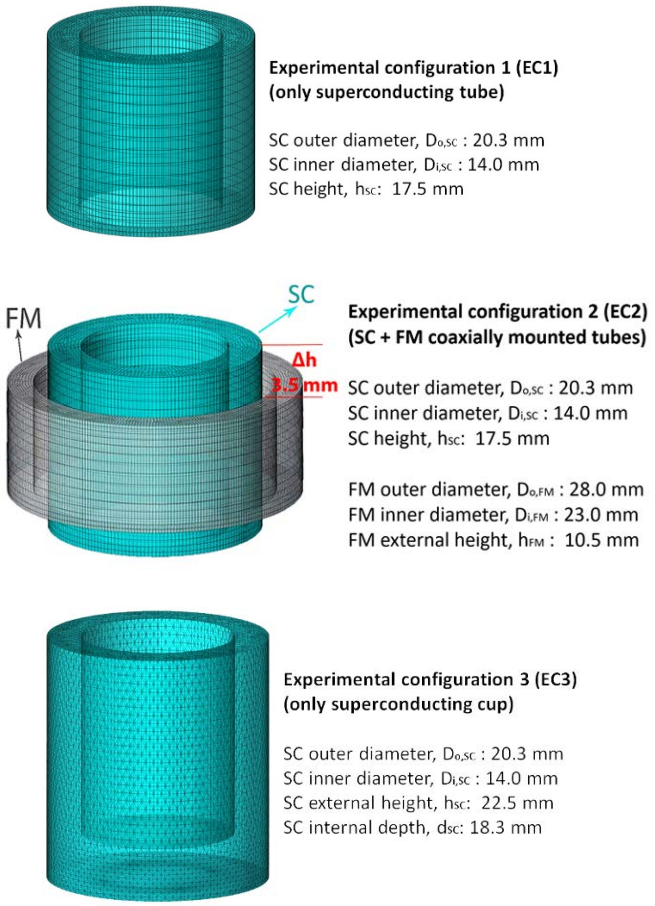

Figure 1. Schematic view of the shielding layouts experimentally tested. From top to bottom: SC hollow cylinder (EC1), SC/FM superimposed hollow cylinders (EC2 - Δh represents the height difference between the edges of the SC/FM hollow cylinders), SC cup (EC3).

3. Modelling

Numerical modelling was implemented by means of the commercial finite-element software COMSOL Multiphysics® 5.4 [44], assuming the external magnetic field applied either parallel or perpendicular to the shield axis. Note that, addressing the latter configuration strictly requires a 3D approach, which we also extended to the former orientation for consistency.

We used the Magnetic Fields interface (*mf*), suitable for computing magnetic fields and induced currents. It solves Maxwell's equations formulated using the magnetic vector potential **A** for all the domains. The magnetic field of the desired orientation is applied as the boundary condition on a spherical computation box with a diameter of 160 mm. The superconducting domain differs from the rest by introducing a current density, **j**, controlled by the electric field, **E**, following a highly non-linear current-voltage (*I*-*V*) characteristic. As its mathematical form we utilised a hyperbolic tangent, which can be considered a smooth approximation of the step-wise change familiar in the critical state model [48]. Such a form also resulted from the microscopic analysis in Campbell's original paper [49] suggesting the use of the magnetic vector potential (**A**) formulation to describe the flux dynamics in hard superconductors. Its suitability for modelling the magnetization in objects combining superconductors and magnetic materials in the Coulomb gauge is well documented [42, 50], as long as there is a neutral zone in the superconductor where the current density is zero and the magnetic flux penetrates monotonically from the sample surface when the applied field increases monotonically. Very recently this formulation has been extended to solve 3D problems [45].

In 3D the working equation for the current density flowing in a superconductor must introduce the relation between electric field and current respecting the vector character of both these fields. Assuming the isotropy of the superconductor properties, i.e. that the current density vector of is always co-linear with the electric field vector, leads to the expression:

$$\boldsymbol{j} = j_c tanh\left(\frac{|E|}{E_0}\right)\left(\frac{E_x}{|E|}\boldsymbol{u_x} + \frac{E_y}{|E|}\boldsymbol{u_y} + \frac{E_z}{|E|}\boldsymbol{u_z}\right) \qquad (1)$$

being $(E_x, E_y, E_y) = \left(-\frac{\partial A_x}{\partial t}, -\frac{\partial A_y}{\partial t}, -\frac{\partial A_z}{\partial t}\right)$ the local value of the electric field, E_0 the threshold electric field used to define the critical current density (here assumed to be equal to 10^{-4} V/m) and j_c the *local* critical current density ($j_c \geq \sqrt{j_x^2 + j_y^2 + j_z^2}$). $\boldsymbol{u_x}$, $\boldsymbol{u_y}$ and $\boldsymbol{u_z}$ are the unit vectors along the *x*-, *y*- and *z*-directions, respectively. Equation (1) slightly differs from the relation discussed in [45], which provided an imperfect isotropy for weak electric fields.

According to [37] and [33], we assumed the following j_c dependence on the magnetic field:

$$j_c(B) = j_{c,0}\, exp\left[-\left(\frac{|B|}{B_0}\right)^{\gamma}\right] \qquad (2)$$

where $j_{c,0}$, B_0 and γ are fit parameters. Their values were obtained from the experimental J_c curves in turn calculated from the magnetic flux density cycles measured by the Hall probes [12, 33].

The magnetic properties of the FM material were defined by the interpolation of the magnetic flux density versus the applied field curve measured experimentally on a small piece of the ARMCO iron and reported in the appendix. In the investigated range of temperature, their temperature dependence is negligible. Also, the electrical conductivity of the iron, here set to $2{\cdot}10^4$ S/m, was proved to affect the shielding factor of the hybrid shield in a negligible way.

The source term for the applied magnetic field, $\mathbf{H_{appl}}$, was

taken into account through the boundary conditions: at a large distance from the shield(s), the magnetic flux density, **B**, was assumed to be constant and equal to $\mu_0\mathbf{H}_{\mathbf{appl}}$. All the calculations were carried out assuming a quasi-static field condition with a rising rate of $\frac{\mathrm{d}(\mu_0 H_{\mathrm{appl}})}{\mathrm{d}t} = 0.35$ T/s of the applied field. The same results could have been achieved by decreasing both the rising rate and E_0 in equation (1) by the same factor, but at the cost of longer computation time. On the other hand, it is worth mentioning that $E_0 = 10^{-4}$ V/m is a conventional value usually chosen in the electrical transport measurements and lower E_0 values was predicted in magnetic measurements where the applied field is swept slowly [51].

4. Experimental verification of the modelling method

Figure 2 shows the values of the magnetic flux density measured at fixed positions on the axis of the hollow cylinder EC1 in both axial (AF) and transverse (TF) field orientations at T = 30 K. The experimental data are compared with those calculated in the same positions with the modelling procedure described in Sect. 3. In agreement with [33], to describe the $j_c(B)$ dependence of the superconductor at this temperature, the following parameters were employed in (2): $j_{c,0} = 3.01 \cdot 10^8$ A/m^2, $B_0 = 0.83$ T and $\gamma = 2.52$. For both the applied field orientations, the computed shielding performance well reproduced the experimental data.

Then, the comparison was carried out on the hybrid SC/FM configuration EC2 where the superconducting hollow cylinder and Hall probe locations are the same as in EC1. As can be seen in figure 3, the superimposition of a ferromagnetic shield does not compromise the remarkable agreement between experiment and calculation.

Lastly, we calculated the magnetic flux density along the axis of a superconducting cup (shielding configuration EC3). In order to liken these computation outputs to the experimental ones reported in [12], the parameters $j_{c,0} = 5.02 \cdot 10^8$ A/m^2, $B_0 = 0.98$ T and $\gamma = 3.78$ were introduced in (2). These values were obtained by fitting the experimental

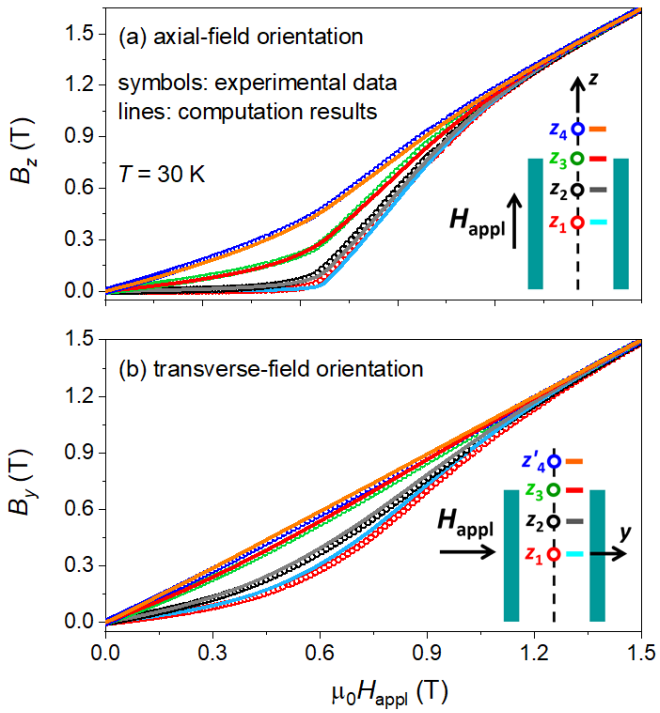

Figure 2. Comparison between (a) B_z values measured in the AF orientation and (b) B_y values measured in the TF orientation at T = 30 K by Hall probes located along the axis of the SC hollow cylinder EC1 and the corresponding curves computed by numerical simulations. In the shield scheme, the circles indicate the Hall probe positions and the solid lines the corresponding computed curves. Assuming $(x,y,z) = (0,0,0)$ the coordinate of the shield center, in the AF orientation the Hall probes were positioned at $z_1 = 0$ mm, $z_2 = 4.4$ mm, $z_3 = 8.8$ mm (shield edge coordinate) and $z_4 = 13.1$ mm. In the transverse-field orientation, the Hall probes were placed at the same positions, except $z'_4 = 12.0$ mm.

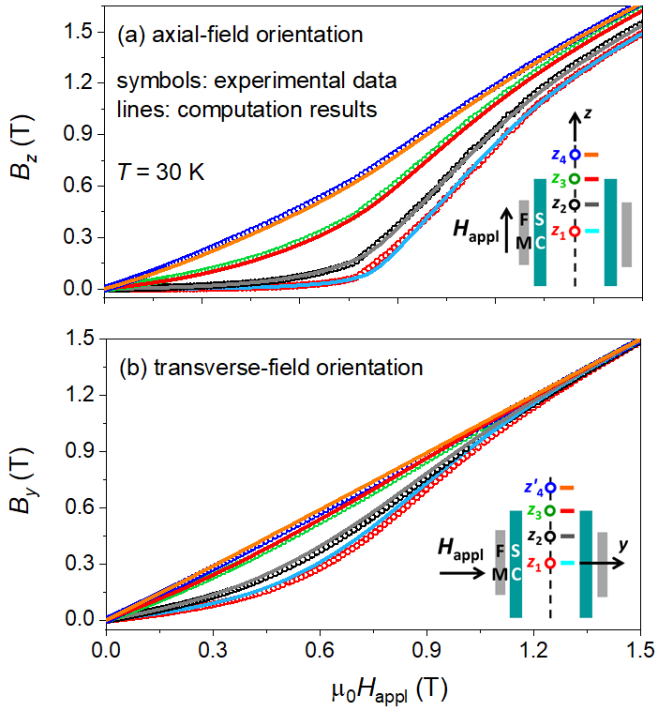

Figure 3. Comparison between (a) B_z values measured in the AF orientation and (b) B_y values measured in the TF orientation at T = 30 K by Hall probes located along the axis of the hybrid SC/FM tubular shield EC2 and the corresponding curves computed by numerical simulations. In the shield scheme, the circles indicate the Hall probe positions and the solid lines the corresponding computed curves. Assuming $(x,y,z) = (0,0,0)$ the coordinate of the shield centre, in the AF orientation the Hall probes were positioned at $z_1 = 0$ mm, $z_2 = 4.4$ mm, $z_3 = 8.8$ mm (SC shield edge coordinate) and $z_4 = 13.1$ mm. In the transverse-field orientation, the Hall probes were placed at the same positions, except $z'_4 = 12.0$ mm.

$J_c(\mu_0 H_{appl})$ curve measured in [12] at 30 K by equation (2), where $|B|$ was replaced by $\mu_0 H_{appl}$. According to the procedure discussed in [33], the fit was limited to the range of applied fields greater than the full penetration field. Then, the resulting fit parameters were assumed effective in defining $j_c(B)$ in the whole investigated range of applied fields.

The comparison between experimental and calculated magnetic flux density is reported in figure 4 and it evidences a valuable correspondence here as well. However, the calculation cannot reproduce the flux jump occurrence [52, 53] at $\mu_0 H_{appl}$ = 1.0 T. This finding was expected considering that our model predicts a homogeneous field penetration. Based on the outcomes of [54, 55], a model upgrading is ongoing, but this issue is beyond the aim of this paper. In addition, there is some discrepancy in the TF orientation when the applied field overcomes $\mu_0 H_{appl}$ = 0.9 T, *i.e.* when the magnetic flux starts entering the cup also through the closed extremity. This could be due to the fact that the inner surface of the cup base is not exactly flat. At the present stage, we find it counterproductive to introduce this roughness into the numerical model because it will significantly increase the model complexity. Moreover, we expect minor model improvement from this manipulation.

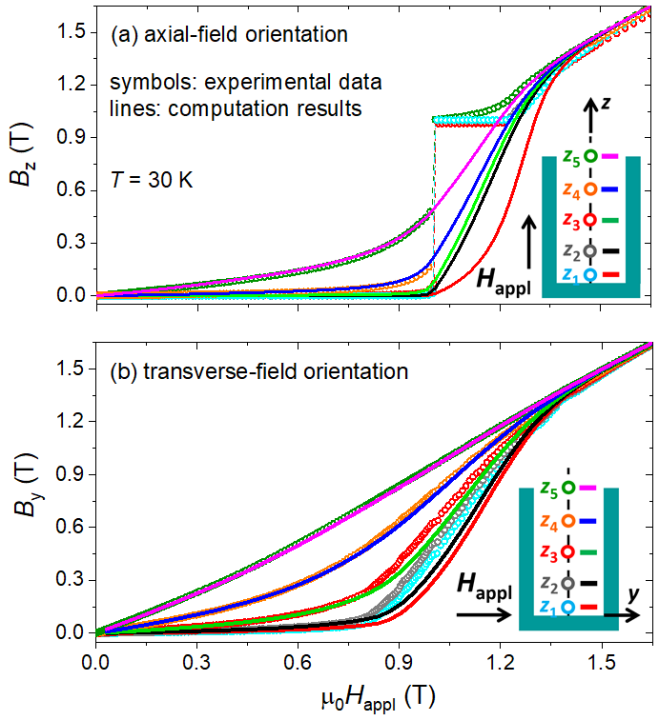

Figure 4. Comparison between (a) B_z values measured in the AF orientation and (b) B_y values measured in the TF orientation at T = 30 K by Hall probes located along the axis of the SC cup-shaped shield EC3 and the corresponding curves computed by numerical simulations. Circles indicate the Hall probe positions in the experiments. Assuming (x,y,z) = (0,0,0) the coordinate of the closed extremity, in the AF orientation the Hall probes were positioned at z_1 = 1.0 mm, z_2 = 5.0 mm, z_3 = 9.2 mm (shield's centre), z_4 = 13.7 mm, and z_5 = 18.3 mm (shield's open extremity). In the transverse-field orientation, the Hall probes were placed at the same positions.

5. Shielding performances of superconducting and ferromagnetic coaxial cups

The comparison between the shielding factors measured along the main axis of the arrangements EC1 and EC2 highlighted the effective role of the FM hollow cylinder addition in widening the region where high shielding factors are achieved (figure 5). In the TF orientation, this enlargement is complemented by a better shielding in the whole investigated field range, while for the AF orientation it is at the cost of a minor worsening of the shielding performance at low fields. Here, the shielding factor is defined as the ratio of the applied magnetic field, $\mu_0 H_{appl}$, to the magnitude of the local magnetic flux density, B.

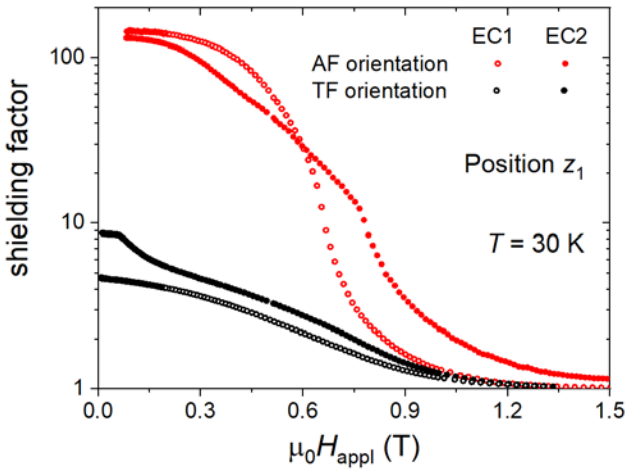

Figure 5. Comparison between the shielding factors measured in both axial- and transverse-field orientations at T = 30 K by the Hall probes positioned in the shield centre for the superconducting shield EC1 (open symbols) and hybrid shield EC2 (solid symbols).

On the other hand, we already proved, both by computation [33] and experiment [12], how the addition of a cap (disk) on one of the tube apertures strongly improve the SFs in axial applied fields. Likewise, when the cap and the tube are 'fused' together with no gap in between, a similar improvement was predicted also in transverse applied fields [29]. Notably, the dependence of the shielding properties on the wall thickness of the SC shield is not addressed here, because it was predicted not to be a crucial parameter in short bulk shield with field-dependent J_c [56, 33].

Based on these outcomes, we focused on cup-shaped shields and investigated how the SF of a SC cup is modified by superimposing a coaxial FM cup on it. The study was carried out as a function of the height of the FM cup (figure

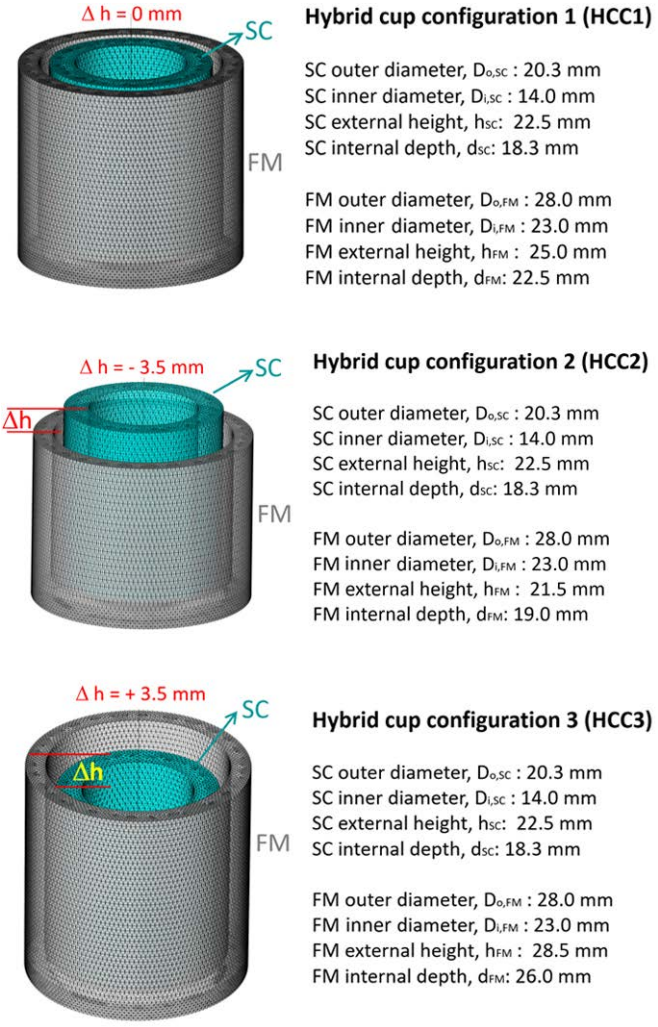

Figure 6. Schematic view of the layouts whose shielding properties were calculated. From top to bottom: SC/FM superimposed cups with the open extremity at the same height (HCC1 - Δh represents the height difference between the cups' edges), SC/FM superimposed cups with SC cup protruding above the FM one (HCC2) and SC/FM superimposed cups with FM cup protruding above the SC one (HCC3).

6), in both axial-field and transverse-field orientations, assuming that the size and the physical properties of the SC cup are the same as of cup EC3. The FM cup was considered to be made out of Fe ARMCO with the same *B-H* constitutive law as the FM tube characterized experimentally (figure A1).

As can be seen in figure 7, the addition of the FM cup induced a worsening in the shielding ability at low applied fields. This can be explained by the fact that in such short shields the entering of the magnetic flux from the cup opening is predominant. Therefore, the presence of a greater magnetic flux density at the shield opening, caused by the FM component that attracts the magnetic flux lines, affects the SF throughout the shield. However, this SF worsening was partially mitigated when the open edges of the two cups are at a different level.

Conversely, at higher magnetic fields, when the flux penetration from the walls becomes significant, the addition of the FM widens the range of applied fields where elevated shielding factors can be achieved. Configuration HCC3 is the most efficient providing SF higher than 10^2 in the whole inner half of the SC cup up to $\mu_0 H_{appl}$ = 1.1 T.

The shielding factors calculated in the transverse-field orientation for the same shielding configurations are plotted in figure 8 as a function of the applied field. In contrast to what was observed in the axial-field orientation, the addition of the FM hollow cylinder improved the shielding factor of the structure in the whole investigated range of applied fields. The range of external fields displaying the highest SFs corresponds to that in which for no zones of the ferromagnetic shell the magnetic flux density overcomes the saturation values. In this range, the aspect ratio of the FM cup strongly influences the shielding ability of the whole structure.

Notably, at $\mu_0 H_{appl}$ = 0.1 T, the SF predicted for HCC3 is more than 8 times greater than that calculated for EC3 almost in the whole volume inside the superconducting cup, as evidenced by the SF maps in the *yz* and *xz* planes (namely, in planes parallel and perpendicular to the applied field

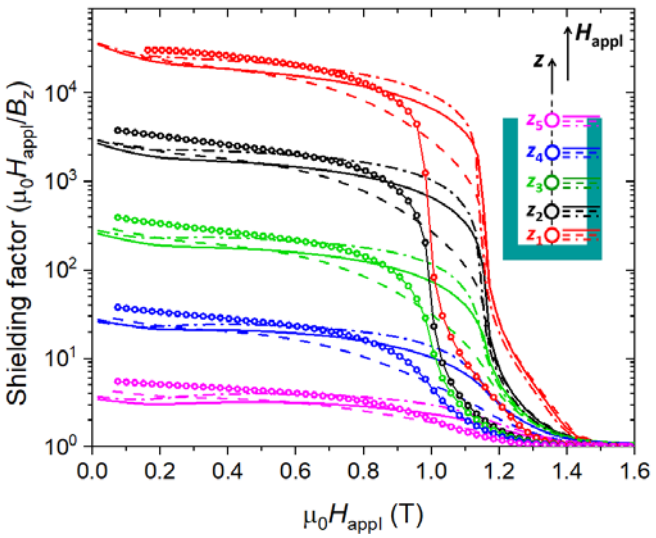

Figure 7. Comparison between the shielding factors calculated in the axial-field orientation for the cup configurations EC3 (open symbols), HCC1 (solid line), HCC2 (dashed line), HCC3 (dashed-dotted line). The values shown in the figure were computed along the shield axis, at the same positions as in figure 4. In all calculations, the working temperature of 30 K was assumed and the parameters $j_{c,0}$ = 5.02·10^8 A/m^2, B_0 = 0.98 T and γ = 3.78 was introduced in equation (2) to consider the critical current dependence on magnetic field.

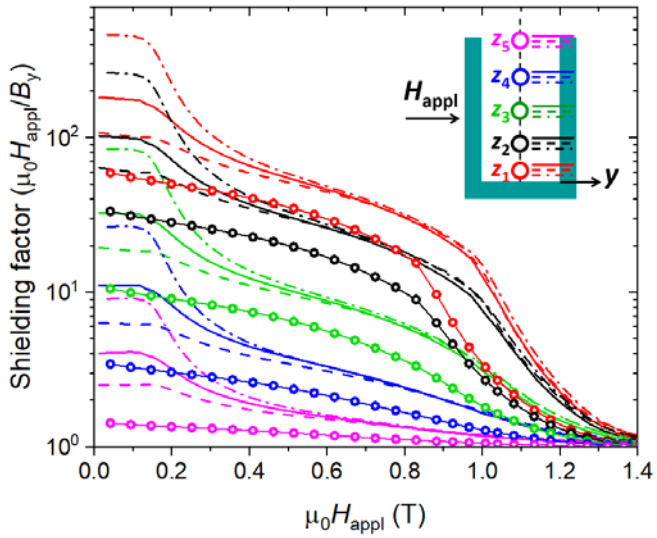

Figure 8. Comparison between the shielding factors calculated in the transverse-field orientation for the cup configurations EC3 (open symbols), HCC1 (solid line), HCC2 (dashed line), HCC3 (dashed-dotted line). The values shown in the figure were computed along the shield axis, at the same positions as in figure 4. In all calculations, the working temperature of 30 K was assumed and the parameters $j_{c,0}$ = 5.02·10^8 A/m^2, B_0 = 0.98 T and γ = 3.78 was introduced in equation (2) to consider the critical current dependence on magnetic field.

direction, respectively) shown in figure 9. This results in a SF increase from 50 to 450 at position z_1 and leads to SFs higher than 100 in about half of the internal volume of the hybrid shield HCC3.

Significant enhancements, although not so high, were obtained with the other two hybrid arrangements with smaller aspect ratios of height/average diameter (SF_{HCC1} $SF_{HCC1}/SF_{EC3} > 3$ and $SF_{HCC2}/SF_{EC3} \sim 2$ at $\mu_0 H_{appl}$ = 0.1 T and $z \leq z_4$). This difference accounts for the diverse magnetic flux lines organization near the open edges of the hybrid shield caused by the different height of the FM cups (figure 10). The last parameter is then crucial in determining the efficiency of the hybrid shield. Conversely, almost negligible changes in the SF of these hybrid layouts were achieved if the FM wall thickness is increased/decreased even by 20% (not shown).

The improvement achieved by the addition of the FM shell can be explained by considering the shielding properties of a ferromagnetic sheet in a transverse field. Indeed, contrary to superconductors [29], long tubular shields of high-permeability materials are expected to mitigate transverse magnetic fields more effectively than axial ones [57], and significant SF improvements was predicted in a transverse field for an ideal rectangular-shaped superconducting shield with an outer layer of μ-metal [58].

Raising above $\mu_0 H_{appl}$ = 0.2 T, some zones of the FM shield reach the magnetic saturation (namely, the outer layer of the closure cap and the last part of the lateral wall in correspondence of the open edge) and the advantage in superimposing the FM shell starts reducing. At

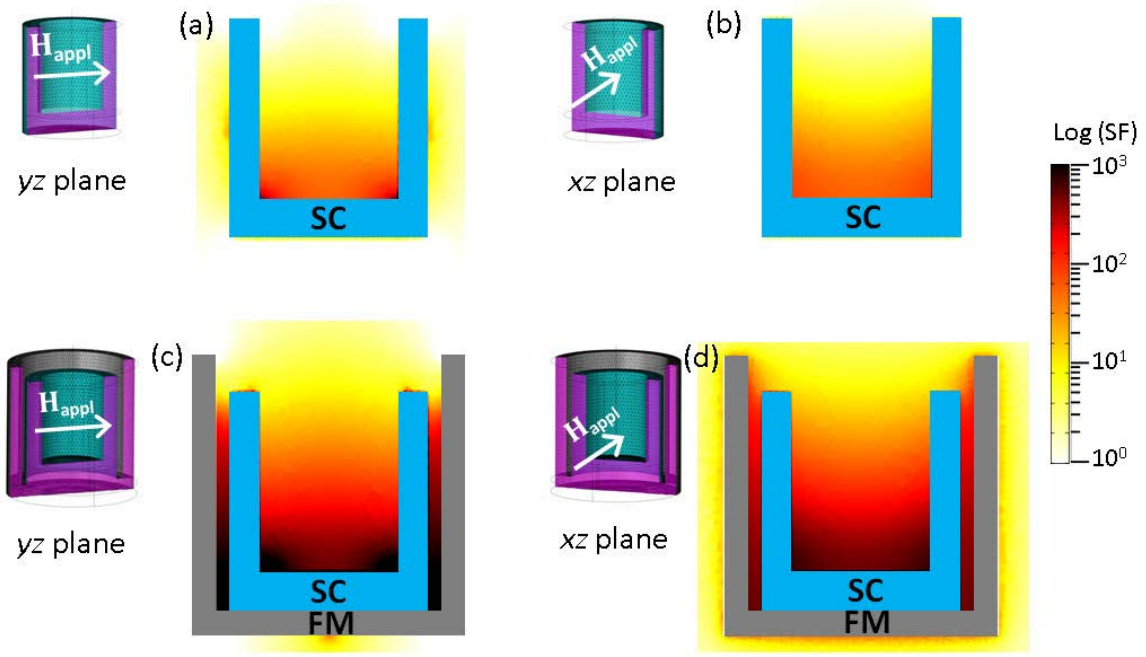

Figure 9. Comparison between the cross-sections in the *yz* (a),(c) and *xz* (b),(d) planes of shields EC3 (a), (b) and HCC3 (c),(d) showing the shielding factor after the external field, applied along the *y* -direction, was ramped up to $\mu_0 H_{appl}$ = 0.1 T. To better represent the full range of the SF values a logarithmic colour scale was used.

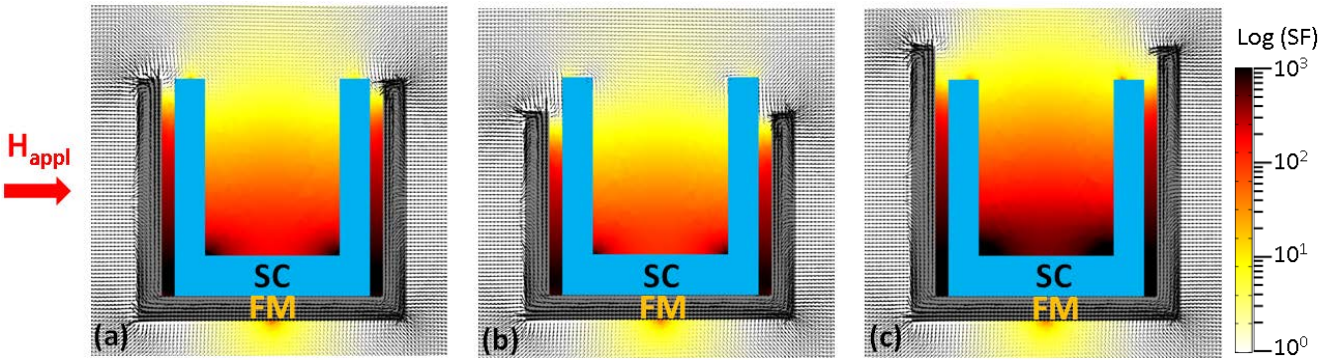

Figure 10. Comparison between the shielding factor (colour) maps and the magnetic flux line distributions computed for shields HCC1 (a), HCC2 (b) and HCC3 (c) after the external field, applied along the *y* -direction, was ramped up to $\mu_0 H_{appl}$ = 0.1 T. Data are related to the cross-sections in the *yz* plane. To better represent the full range of the SF values a logarithmic colour scale was used.

$\mu_0 H_{appl}$ = 0.6 T the SF curves of the three hybrid layouts collapse, becoming independent from the height of the FM cups. However, the persistence of not fully saturated zones in the lateral wall of the FM cup still lowers the external field actually applied to the SC cup and then shifts the SF of the whole shield to greater values than for cup EC3.

6. Conclusions

In this paper, we investigated the shielding properties of short superconducting and hybrid screens with cylindrical symmetry exploiting a 3D modelling approach based on the **A**-formulation of the magnetic field. The analysis was carried out in both axial- and transverse-field orientations, implementing the model in a commercial finite element code.

The feasibility of this model in evaluating the magnetic mitigation of quasi-static magnetic fields was checked by comparing the computed outcomes to experimental results obtained for different MgB_2 and MgB_2/soft-iron cylindrical shields. The good agreement that came out of this analysis evidenced that the model allows a reliable SF evaluation when a uniform field penetration inside the superconductor is expected.

The as-validated numerical procedure was then applied to predict the screening ability of new hybrid shield layouts consisting of SC and FM coaxial cups, with the same physical properties as the shields characterized experimentally.

Calculations highlighted that, at low fields, the superimposition of a FM cup on a SC one partially recovers the performance loss of the SC cup in the TF orientation, thus making these compact hybrid arrangements suited in shielding from both axial and transverse external magnetic fields. The SF worsening induced in the AF orientation can indeed be minimized by the presence of a mismatch, Δh, between the edges of the SC and FM cups, as evidenced by the comparison of the three hybrid configurations differing in this parameter.

In addition, the presence of the external FM shield reduces the magnetic flux density at the superconductor lateral/bottom external walls, enlarging the applied field range where higher SF can be achieved. Finally, a very important outcome of our investigation is the evident need of a 3D approach in numerical modelling of the magnetic mitigation properties of FM/SC hybrid layouts. Indeed, limiting the analysis to a 2D axisymmetric study in AF orientation would have provided incomplete information on the benefit of the FM shield addition at low magnetic fields. This is especially the case of shielding systems with a height/diameter small ratio, where the SF cannot be obtained as a trivial combination of the SF of their components.

Considering the calculation results at low and high applied fields and in both AF and TF orientations, the layout HCC3 with the FM cup protruding over the SC one turns out to be the most promising geometry. Assuming a working temperature of 30 K, at applied fields up to 0.15 T it provides SFs higher than 500 near the close extremity, independently from the field orientation, while in the most favourable AF orientation, a SF $\geq 10^4$ occurs up over 1 T. Starting from the present results, design refinements are under study to further optimize the shielding performance.

Acknowledgements

This article is partially based upon work from COST Action CA19108, supported by COST (European Cooperation in Science and Technology).

The research was supported by the Slovak Research and Development Agency under contract no. APVV-16-0418.

Romanian team acknowledges UEFISCDI, Romania, through Core Program PN19-03 (contract no. 21 N/08.02.2019) and the projects POC 37_697 no.

28/01.09.2016 REBMAT and PNIII-P1-1.1-PD-2019-0651 SUPRASHAPE.

Appendix

In all the calculations, the ferromagnetic shells were supposed to be made out of iron ARMCO whose *B–H* characteristic curve is plotted in figure A1. Fe ARMCO was proved to have negligible hysteresis losses: therefore, we did not consider this parameter in modelling. Its relative permeability at low fields overcomes the value μ_r = 7500, while its saturation magnetic flux density is ~ 2.3 T.

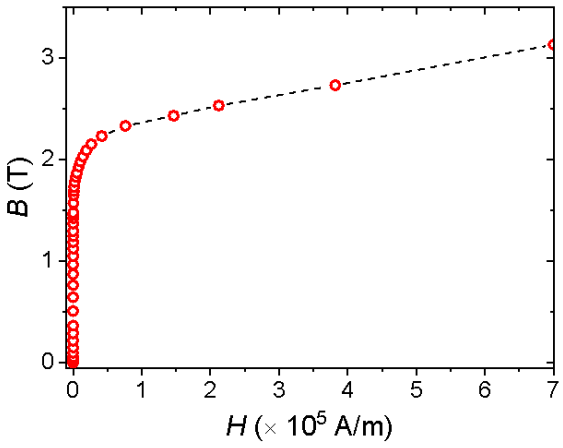

Figure A1. *B–H* characteristic curve of the iron ARMCO used for modelling the FM shells.

References

[1] Denis S, Dusoulier L, Dirickx M, Vanderbemden P, Cloots R, Ausloos M and Vanderheyden B 2007 *Supercond. Sci.Technol.* **20** 192–201

[2] Terao Y, Sekino M, Ohsaki H, Teshima H and Morita M 2011 *IEEE Trans. Appl. Supercond.* **21** 1584-7

[3] Wéra L, Fagnard J F, Levin G A, Vanderheyden B and Vanderbemden P 2015 *Supercond. Sci. Technol.* **28** 074001

[4] Nagasaki Y, Solovyov M and Gömöry F, 2018 *IEEE Trans. Appl. Supercond.* **28** 6601905

[5] Kvitkovic J, Patel S, Zhang M, Zhang Z, Peetz J, Marney A and Pamidi S 2018 *IEEE Trans. Appl. Supercond.* **28** 9001705

[6] Yang P, Fagnard J F, Vanderbemden P and Yang W 2019 *Supercond. Sci. Technol Supercond. Sci. Technol.* **32** 115015

[7] Chi C, Cai C, Zhou D, Guo Y, Yan W, Bai C, Liu Z, Lu Y, Fan F, Li M and Zeng Z 2020 *Supercond. Sci. Technol Supercond. Sci. Technol.* **33** 095001

[8] Dorget R, Nouailhetas Q, Colle A, Berger K, Sudo K, Ayat S, Lévêque J, Koblischka M F, Sakai N, Oka T and Bruno Douine 2021 *Materials* **14** 2847

[9] Bortot L, Mentink M, Petrone C, Van Nugteren J, Deferne G, Koettig T, Kirby G, Pentella M, Perez J C, Pincot F O, De Rijk G, Russenschuck S, Verweij A P and Schöps S 2021 *Supercond. Sci Technol* **34** 105001

[10] Wéra L, Fagnard J -F, Namburi D K, Shi Y, Vanderheyden B and Vanderbemden P 2017 *IEEE Trans. Appl. Supercond.* **27** 6800305

[11] Giunchi G, Barna D, Bajas H, Brunner K, Német A and Petrone C 2018 *IEEE Trans. Appl. Supercond.* **28** 6801705

[12] Gozzelino L, Gerbaldo R, Ghigo G, Torsello D, Bonino V, Truccato M, Grigoroscuta M A, Burdusel M, Aldica G V, Sandu V, Pasuk I and Badica P 2020 *Supercond. Sci. Technol.* **33** 044018

[13] Omura A, Oka M, Mori K and Itoh M 2003 *Physica C* **386** 506–11

[14] Seki Y, Suzuki D, Ogata K and Tsukada K 2003 *Appl. Phys. Lett.* **82** 940–2

[15] Lousberg G P, Fagnard J-F, Ausloos M, Vanderbemden P and Vanderheyden B 2010 *IEEE Trans. Appl. Supercond.* **20** 33–41

[16] Gozzelino L, Agostino A, Gerbaldo R, Ghigo G and Laviano F 2012 *Supercond. Sci. Technol.* **25** 115013

[17] Kvitkovic J, Patel S and Pamidi S 2017 *IEEE Trans. Applied Supercond.* **27** 4700705

[18] Gozzelino L, Gerbaldo R, Ghigo G, Laviano F, Truccato M 2017 *J Supercond Nov Magn* **30** 749-56

[19] Fareed M U and Ruiz H S 2021 *Materials* **14** 6204

[20] Gömöry F, Solovyov M, Šouc J, Navau C, Prat-Camps J and Sanchez A 2012 *Science* **335** 1466–8

[21] Gömöry F, Solovyov M and Šouc J 2015 *Supercond. Sci. Technol.* **28** 044001

[22] Prat-Camps J, Navau C and Sanchez A 2015 *Sci. Rep.* **5** 12488

[23] Zhou P-B, Ma G-T, Wang Z-T, Gong T-Y, Ye C-Q and Zhang H 2016 *IEEE Trans. Appl. Supercond.* **26** 0601805

[24] Capobianco-Hogan K G, Cervantes R, Deshpande A, Feege N, Krahulik T, LaBounty J, Sekelsky R, Adhyatman A, Arrowsmith-Kron G, Coe B, Dehmelt K, Hemmick T K, Jeffas S, LaByer T, Mahmud S, Oliveira A, Quadri A, Sharma K and Tishelman-Charny S 2018 *Nucl. Instrum. Methods Phys. Res. A* **877** 149-56

[25] Rabbers J J, Oomen M P, Bassani E, Ripamonti G and Giunchi G 2010 *Supercond. Sci. Technol.* **23** 125003

[26] Giunchi G 2014 *Proc. of the 20th IMEKO TC4 Symp. On Measurements of Electrical Quantities* (Budapest: IMEKO) pp 1020–4.

[27] Prouvé T, Duval J M, Luchiera N and D'escrivan S, 2014 *Cryogenics* **64** 201-6

[28] Hogan K, Fagnard J-F, Wéra L, Vanderheyden B and Vanderbemden P 2018 *Supercond. Sci. Technol.* **31** 015001

[29] Fagnard J F, Vanderheyden B, Pardo E and Vanderbemden P 2019 *Supercond. Sci. Technol.* **32** 074007

[30] Giunchi G, Ripamonti G, Cavallin T and Bassani E 2006 *Cryogenics* **46** 237-40

[31] Bhagurkar A G, Yamamoto A, Anguilano L, Dennis A R, Durrell J H, Hari Babu N and Cardwell J H 2016 *Supercond. Sci. Technol.* **29** 035008

[32] Barna D, Giunchi G, Novák M, Brunner K, Német A, Petrone C, Atanasov M, Bajas H and Feuvrier J 2019 *IEEE Trans. Appl. Supercond.* **29** 4101310

[33] Gozzelino L, Gerbaldo R, Ghigo G, Laviano F, Torsello D, Bonino V, Truccato M, Batalu D, Grigoroscuta M A, Burdusel M, Aldica G V and Badica P 2019 *Supercond. Sci. Technol.* **32** 034004

[34] Campbell A M 2014 *Supercond. Sci. Technol.* **27** 124006

[35] Grilli F, Pardo E, Stenvall A, Nguyen D N, Yuan W and Gömöry F 2014 *IEEE Trans. Appl. Supercond.* **24** 8200433

[36] Sirois F and Grilli F 2015 *Supercond. Sci. Technol.* **28** 043002

[37] Ainslie M D and Fujishiro H 2015 *Supercond. Sci. Technol.* **28** 053002

[38] Prigozhin L and Sokolovsky V 2018 *Supercond. Sci. Technol.* **31** 055018
[39] Shen B, Grilli F and Coombs T 2020 *IEEE Access* **8** 100403
[40] Berrospe-Juarez E, Trillaud F, Zermeño V M R and Grilli F 2021 *Supercond. Sci. Technol.* **34** 044002
[41] Arsenault A, Sirois F and Grilli F 2021 *IEEE Trans. Appl. Supercond.* **31** 6800609
[42] Gömöry F, Vojenčiak M, Pardo E and Šouc J 2009 *Supercond. Sci. Technol.* **22** 034017
[43] Gozzelino L, Gerbaldo R, Ghigo G, Laviano F, Truccato M and Agostino A 2016 *Supercond. Sci. Technol.* **29**, 034004
[44] COMSOL Multiphysics® (https://www.comsol.com/).
[45] Solovyov M and Gömöry F 2019 *Supercond. Sci. Technol.* **32** 115001.
[46] Gozzelino L, Gerbaldo R, Ghigo G, Laviano F, Agostino A, Bonometti E, Chiampi M, Manzin A, and Zilberti L 2013 *IEEE Trans. Appl. Supercond.* **23,** 8201305
[47] Gozzelino L, Minetti B, Gerbaldo R, Ghigo G, Laviano F, Agostino A and Mezzetti E 2011 *IEEE Trans. Appl. Supercond.* **21** 3146-9
[48] Bean C P 1962 *Phys. Rev. Lett.* **8** 250-3
[49] Campbell A M 2007 *Supercond. Sci. Technol.* **20** 292–5
[50] Gömöry F, Vojenčiak M, Pardo E, Solovyov M, Šouc J 2010 *Supercond. Sci Technol.* **23** 034012
[51] Golovchanskiy I A, Pan A V, Shcherbakova O V, and Fedoseev S A 2013 *J. Appl. Phys.* **114** 163910
[52] Romero-Salazar C, Morales F, Escudero R, Durán A and Hernández-Flores O A 2007 *Phys. Rev. B* **76** 104521
[53] Ghigo G,Gerbaldo R, Gozzelino L, Laviano F, Lopardo G, Monticone E, Portesi C and Mezzetti E 2009 *Appl. Phys. Lett.* **94** 052505
[54] Hirano T, Fujishiro H, Naito T and Ainslie M D 2020 *Supercond. Sci. Technol.* **33** 044003
[55] Cientanni V and Ainslie M D presented at Applied Superconductivity Conference 2020.
[56] Niculescu H, Schmidmeier R, Topolscki B and Gielisse P 1994 Physica C 299 105–12
[57] Filtz M and Büssing H 2008 *Electr. Eng.* **90** 469-78
[58] Claycomb J R 2016 in "Applied Superconductivity - Handbook on Devices and Applications", edited by P Seidel, (Weinheim:Wiley-VCH Verlag GmbH & Co. KGaA) pp. 780-806